Professor Blair Perot
Department of Mechanical Eng.
University of Massachusetts
Amherst, MA 01003
Phone: (413) 545-3925
Fax: (413) 545-1027
perot@ecs.umass.edu

Turbulence Modeling Using Body Force Potentials

Blair Perot
Department of Mechanical Engineering
University of Massachusetts, Amherst, MA 01003

Abstract

Reynolds Averaged Navier-Stokes (RANS) turbulence models are usually concerned with modeling the Reynolds stress tensor. An alternative approach to RANS turbulence modeling is described where the primary modeled quantities are the scalar and vector potentials of the turbulent body force - the divergence of the Reynolds stress tensor. This approach is shown to have a number of attractive properties, most important of which is the ability to model non-equilibrium turbulence situations accurately at a cost and complexity comparable to the widely used two-equation models such as k-ε.

Like Reynolds stress transport equation models, the proposed model does not require a hypothesized constitutive relation between the turbulence and the mean flow variables. This allows non-equilibrium turbulence to modeled effectively. However, unlike Reynolds stress transport equation models, the proposed system of partial differential equations is much simpler to model and compute. It involves fewer variables, no realizability conditions, and removes the strong coupling between the equations. A detailed analysis of the turbulent body force potentials and their physical significance reveals that they represent the relevant information contained in the Reynolds stress tensor and are fundamental turbulence quantities in their own right.

Model predictions for a number of basic turbulent flows are presented including: channel flow at various Reynolds numbers, mixing layer, rotating channel flow, adverse pressure gradient boundary layers, low Reynolds number backward facing step, and transition to turbulence in channel flow.

PACS: 47.27.Ak, 47.27.Eq, 47.27.Jv

Introduction

Engineering predictions of turbulent flow rely heavily on the Reynolds Averaged Navier-Stokes (RANS) equations. The RANS equations, which look very similar to the original governing Navier-Stokes equations, describe the behavior of the mean flow. This greatly reduces the computational expense of solving the equations since small temporal and spatial scales associated with the turbulence are not resolved. However, averaging the Navier-Stokes equations to obtain the RANS equations removes some information from the system and the RANS equations are not closed. RANS models come in a wide variety of forms. Each attempts to close the system in some physically realistic way, with the more complex models hopefully representing more of the underlying turbulence physics.

For incompressible, isothermal flow the Reynolds Averaged Navier-Stokes equations take the form,

$$\frac{\partial \mathbf{u}}{\partial t} + \nabla \cdot (\mathbf{uu}) = -\nabla p + \nabla \cdot \nu \nabla \mathbf{u} - \nabla \cdot \mathbf{R} \qquad (1a)$$

$$\nabla \cdot \mathbf{u} = 0 \qquad (1b)$$

where $\mathbf{u}$ is the mean velocity vector, p is the mean pressure/density, ν is the kinematic viscosity, and $\mathbf{R} = \overline{\mathbf{u'u'}}$ is the Reynolds stress tensor. The Reynolds stress tensor is the correlation of the fluctuating velocity components and represents the crucial unknown in these equations. The fundamental goal of RANS models is to hypothesize a relationship between this tensor and the mean flow variables so that Eqns. (1a) and (1b) can be solved. The same principals exist for the general (compressible) RANS equations, but we will restrict our attention to the incompressible case here and throughout this document for the sake of simplicity.

Many RANS models assume a constitutive algebraic relation between the Reynolds stress tensor and the mean flow gradients. The most common relation is the eddy viscosity model, $\mathbf{R} = \frac{2}{3}k\mathbf{I} - \nu_T(\nabla \mathbf{u} + \nabla \mathbf{u}^T)$, where k is the turbulent kinetic energy and ν_T is the eddy viscosity. For incompressible flow k can be absorbed into the pressure and is not required explicitly. This relation is also called the Boussinesq hypothesis or the linear eddy viscosity model. It forms the basis for a wide variety of RANS turbulence models which each differ in how the eddy viscosity is calculated. More complex constitutive relations are certainly possible[1-4] and these nonlinear eddy viscosity relations fix a number of deficiencies of the standard linear model, but they still assume that the turbulence is close to equilibrium and has had time to adjust to any changes in the mean flow. Unfortunately, many turbulent flows of practical engineering significance are not close to equilibrium. A classic example is the adverse pressure gradient boundary layer. Other examples include rapidly strained flows and three-dimensional boundary layers. In fact, Lund & Novikov[5] have shown (using direct numerical simulation data) that, in general, an algebraic constitutive relation of arbitrary complexity based on the mean velocity gradients is fundamentally incapable of representing the Reynolds stresses. The equilibrium assumption imbedded in any constitutive relation for the Reynolds stress tensor is emphasized here because the proposed model avoids such a relation and therefore has the potential to predict non-equilibrium turbulent flows more accurately.

There is some prior evidence that models which avoid a constitutive relation for the Reynolds stress tensor outperform other models of the same general class. Both examples of this phenomenon come from models developed for nearly parallel shear flows (where the

Reynolds shear stress is the important Reynolds stress). For example, the zero-equation model of Johnson & King[6] solves an ordinary differential equation for the maximum turbulent shear stress. As a result it generally performs better than other zero-equation models which use the traditional approach of defining an eddy viscosity. A similar result is also obtained with two-equation models. The model of Bradshaw, Ferriss & Atwell[7] was widely accepted to be the most accurate model of the 1968 Stanford competition[8]. This model differed from the competitors in that it solved an equation for the shear stress directly, rather than using a constitutive equation involving the mean shear. The principal drawback of both these methods (and probably the reason that they are not more popular) is that they can only be applied to nearly parallel shear flows. In some sense, the proposed model can be viewed as a way to generalize the two-equation model of Bradshaw *et. al.* to arbitrary flows.

In the past, for arbitrary flows the only alternative to using a constitutive relation was to solve modeled transport equations for the Reynolds stress tensor itself (first proposed by Rotta[9]). Reynolds stress transport models[10-12] can potentially contain more physics than eddy-viscosity based models, however the equations are significantly more difficult to solve. In three dimensions one must solve six highly coupled transport equations for each Reynolds stress. The equations are stiff, and none of the Reynolds stresses are universally dominant, so uncoupling the equations numerically is very difficult. In addition, the Reynolds stress tensor is a positive definite tensor but the modeled equations often do not preserve this property. The proposed model does not suffer from these difficulties. It involves fewer equations than a Reynolds stress transport model. The equations are not strongly coupled and are not as numerically stiff.

The key to developing a model which avoids the use of a constitutive relation and yet does not involve the complexity of a full Reynolds stress transport closure is to note that the Reynolds stresses contain more information than required by the mean flow. Only the divergence of the Reynolds stress tensor (a body force vector) is required to solve for the mean flow. With this in mind, the potential turbulence model defines two new turbulent quantities – the scalar and vector potentials of the body force vector[13]. The advantages of a model that uses these turbulent potentials, rather than the body force vector itself, are twofold. Firstly, this allows the momentum equation to remain a conservative equation. Secondly, and more importantly, these potentials have a very clear physical interpretation which will facilitate the construction of models for their evolution. Turbulence modeling based on the force vector itself (or its rotational component – the Lamb vector) have been proposed by Wu, Zhou & Wu[14], and Marmanis[15], but the author is not aware of any model results based on these ideas.

The properties of the scalar and vector potentials of the turbulent body force (turbulent potentials) are derived in section 2. Exact transport equations for these potentials are derived in section 3 and the unclosed source terms in those equations are then modeled. Section 4 is a short summary of the model and its theoretical properties. Predictions for some basic turbulent flows are presented in Section 5, and a discussion of the major conclusions of this work are found in section 6.

2. Turbulent Potentials

The scalar potential, ϕ, and vector potential, ψ, of the turbulent body force are defined mathematically by the following equations.

$$\nabla\phi + \nabla\times\psi = \nabla\cdot\mathbf{R} \tag{2a}$$

$$\nabla\cdot\psi = 0 \tag{2b}$$

The second equation is a constraint on the vector potential. Other constraints are possible but this is the simplest for the purposes of our analysis. These equations can be rewritten to express the turbulent potentials individually.

$$\nabla^2\phi = \nabla\cdot(\nabla\cdot\mathbf{R}) \tag{3a}$$

$$-\nabla^2\psi = \nabla\times(\nabla\cdot\mathbf{R}) \tag{3b}$$

The boundary conditions on these elliptic equations are prescribed so that the potentials have a real physical interpretation as turbulence quantities. We therefore require that when turbulence is absent, the potentials also vanish. The result is that both potentials are required to go to zero at infinity, at a wall, or at a free surface. The free-surface condition is less intuitive but is consistent with the analysis of flows with a single inhomogeneous direction described below.

Note that by its very definition (Eqn. 2a) the scalar potential is that part of the turbulence that contributes to the mean pressure but does not effect the mean vorticity. Only the vector potential has the ability to effect the mean vorticity, and it only moves the vorticity around (enhanced transport), it does not create or destroy mean vorticity. Physically, we sometimes find it useful to regard the scalar potential as a measure of the average pressure drop in the cores of turbulent vortices, and the vector potential as a measure of the average vorticity magnitude of the turbulent vortices.

In flows with a single inhomogeneous direction (say the y-direction), Eqns. (3a) and (3b) simplify to $\phi = R_{22}$, $\psi_1 = -R_{23}, \psi_2 = 0, \psi_3 = R_{12}$. For this reason, it is also reasonable to view the vector potential as a conceptual generalization of the shear stress ($\overline{u'v'}$) to arbitrary geometries and three dimensions. In nominally two-dimensional flows the vector potential is aligned perpendicular to the flow (like the vorticity) and has only a single nonzero component (ψ_3). The scalar potential (in combination with the turbulent kinetic energy) gives a good indication of the anisotropy of the turbulence and is fundamental to modeling the presence of walls and/or surfaces without using wall functions. These relations will be used later, when evaluating the model predictions against experimental and DNS data for the Reynolds stresses.

In three-dimensional flows the presence of the divergence free constraint on the vector potential means that only two components of the vector potential need to updated. The third can be obtained from the divergence constraint. In fact, in the 3D numerical method recently developed by the author the vector potential is updated at roughly the same computational cost as the scalar potential. Since the k and ε transport equations are also solved with the model, the overall complexity and cost of solving the potential model is a maximum of five transport equations (four in 2D). Coupled with the fact that these equations can solved in an uncoupled fashion and are not particularly stiff, the current model is an order of magnitude faster than Reynolds stress transport equation closures which require updating at least seven coupled equations (five in 2D). However, this reduction in cost sacrifices little, if any, loss in the potential predictive capacity of the model compared to Reynolds stress transport models.

3. Transport Equations for the Turbulent Potentials

Like the Reynolds stress transport equations the exact equations for the evolution of the turbulent potentials can be derived analytically. The connection with Reynolds stress transport models is most clearly understood if the derivation proceeds directly from the Reynolds stress transport equations. In compact notation these equations are written as,

$$\frac{\partial \mathbf{R}}{\partial t} + \mathbf{u}\cdot\nabla\mathbf{R} - \nu\nabla^2\mathbf{R} = \mathbf{P} - \varepsilon + \Pi - \nabla\cdot\mathbf{T} \qquad (4)$$

where $\mathbf{P}$ is the production term, ε is the dissipation tensor, Π is the pressure-velocity gradient correlation tensor and $\mathbf{T}$ is the velocity fluctuation triple correlation. The definition of the last three source terms is not unique, but the cumulative effects of these last three terms must somehow be modeled in order to solve the equations. The corresponding equations for the evolution of the turbulent potentials are,

$$\frac{\partial(\nabla^2\phi)}{\partial t} + \mathbf{u}\cdot\nabla(\nabla^2\phi) - \nu\nabla^2(\nabla^2\phi) = P_\phi + \nabla\cdot\nabla\cdot(-\varepsilon + \Pi - \nabla\cdot\mathbf{T}) \qquad (5a)$$

$$\frac{\partial(\nabla^2\psi)}{\partial t} + \mathbf{u}\cdot\nabla(\nabla^2\psi) - \nu\nabla^2(\nabla^2\psi) = \mathbf{P}_\psi - \nabla\times\nabla\cdot(-\varepsilon + \Pi - \nabla\cdot\mathbf{T}) \qquad (5b)$$

The production terms are no longer directly related to only the turbulent potentials and the velocity gradients. So in flows with more than one direction of inhomogeneity, part of the production terms must be modeled. In turbulent flows with a single direction of inhomogeneity, P_ϕ is zero and $\mathbf{P}_\psi = \nabla^2(\phi\omega)$, where ω is the mean vorticity. In addition, when only one direction of inhomogeneity is present $\nabla\cdot\nabla\cdot(\mathbf{M}) = \nabla^2 M_{22}$ and $-\nabla\times\nabla\cdot(\mathbf{M}) = \nabla^2(-M_{32}, 0, M_{12})$ for any symmetric tensor $\mathbf{M}$. So when one inhomogeneous direction is present the transport equations for the turbulent potentials are identical to the transport equations for the middle column (or row) of the Reynolds stress tensor. The other Reynolds stress components (R_{11}, R_{33}, R_{13}) do not directly influence the mean flow. However, it should be noted that the remaining Reynolds stress can, and probably do, influence the source terms in the transport equations for the turbulent potentials in Eqn. 5. These more subtle effects on the mean flow evolution are accounted for in the model by carrying a transport equation for the turbulent kinetic energy and also the dissipation rate.

While the model includes transport equations for k and ε it should be emphasized that the proposed model is a significant departure from standard two-equation models. These auxiliary quantities are only used to help model the source terms in the turbulent potential evolution equations. They are not used to determine the Reynolds stress tensor and the resulting mean flow. The dissipation rate was chosen for this study because some of the test cases have this quantity available for comparison, but the choice of the particular 'scale' equation is not thought to have a profound effect on the overall performance of the model, since it no longer appears directly in an expression for the Reynolds stresses.

The elimination of the constitutive equation for the Reynolds stresses is an important departure from two-equation models that removes one of the weaker modeling assumptions. In flows with a single inhomogeneous direction (parallel shear flows), the similarity with a Reynolds stress transport model is very clear. The only significant departure is a lumping of the "secondary" Reynolds stresses (those whose gradients do not directly influence the mean flow evolution), into a single quantity – the turbulent kinetic energy. This approach effectively reduces the number of equations in a way which is least likely to impact the mean flow predictions. In addition, it separates the stresses in a meaningful way, allowing the solution of the turbulent transport equations to be numerically uncoupled. As mentioned earlier, this idea of isolating the important Reynolds stresses has been used previously for models restricted to parallel shear flows. However, the turbulent potentials and their evolution equations are well defined in any flow situation and allow one to effectively isolate the most influential parts of the Reynolds stress tensor in any flow geometry.

The general modeling philosophy of this project has been to use existing Reynolds stress transport models, and the assumption of a single inhomogeneous direction, to guide the

construction of the turbulent potential source terms. Other guiding factors have been the construction of a model that naturally obtains the correct asymptotic behavior near walls and free surfaces, and a model which responds correctly to shearing, both initially (rapid distortion theory - RDT) and in the long time limit. Obtaining the correct rapid response for shear flows is important because this situation is closely obtained by many engineering applications. Examples are, free-stream turbulence which suddenly encounters an obstacle (such as a blade in a turbine), and the initial development of tripped boundary layers and free shear layers.

Three principal terms need to be modeled: dissipation, pressure coupling, and turbulent transport. There is some ambiguity in how these terms are defined, but this is of little concern here, since the goal is only to model the respective physical effects. In addition, the effects of system rotation, and transition have also been included. The modeling of each term is described below.

3.1 Dissipation

In Reynolds stress transport models the dissipation tensor is often modeled as an isotropic tensor; the theory being that at high Reynolds numbers small scales should be isotropic. Recent experiments at NASA-Ames by Saddoughi[16] indicate that this hypothesis is probably correct at high enough Reynolds numbers. However, the dissipation rate used in the model is actually an integral over all scales not just small scales. While small scales dominate this integral, recent work[17-18] suggests that the large-scale components can not be neglected in a wide class of flows. Therefore we move to the next level of approximation, where a portion of the dissipation is isotropic and the rest is proportional to the Reynolds stress tensor. Rotta[9] proposed that the dissipation tensor was proportional to the Reynolds stress tensor. It is thought that the Rotta model is the low Reynolds number limit and it has been shown to work quite well near walls[19]. Most dissipation tensor models can be written in the form $\varepsilon = (1-\alpha)\frac{2}{3}\varepsilon\mathbf{I} + \alpha\frac{\varepsilon}{k}\mathbf{R}$, where ε is the dissipation rate of turbulent kinetic energy, and α is some blending parameter. Hanjalic & Launder[20] used a blending factor that was a function of the turbulent Reynolds number. More recently there have been proposals to use a function of a two-componentality factor (which requires the solution of an additional PDE)[21]. In this work we advocate $\alpha = 1/(1+\frac{1.5\phi}{k})$. Such a model has the right near wall and isotropic turbulence limits. In addition it implies that the anisotropy of the dissipation tensor is one half the anisotropy of the Reynolds stress tensor for strained isotropic turbulence, which is the correct rapid distortion limit for both irrotational and rotational mean flows[22].

Assuming either that the inverse turbulent time scale varies slowly or that the flow has a single direction of inhomogeneity gives the following dissipation models, $\varepsilon_\phi = 2\alpha\frac{\varepsilon}{k}\phi$ and $\varepsilon_{\psi_i} = \alpha\frac{\varepsilon}{k}\psi_i$. These models show very good agreement with the DNS data for turbulent channel flow. However, they do not have the correct asymptotic behavior near a wall or a free surface (where $\alpha \to 1$). At a wall the scalar and vector dissipation should go like $4\frac{\varepsilon}{k}\phi$ and $2\frac{\varepsilon}{k}\psi$, respectively. At a free-surface they should go like $\frac{2\nu}{y^2}\phi$ and $O(y)$. The asymptotic order is correct in each case, but the constants are not correct. These constants (along with the pressure redistribution constants) are critical to obtaining the correct asymptotic behavior of the turbulent potentials. Near a wall the potentials go like y^4 and y^3. Obtaining this sort of asymptotic behavior with a single boundary condition (zero potential at the wall) is not a trivial task, and requires that the modeled source terms be exact at the boundary.

Fortunately, a dissipation model that is exact at walls and free-surfaces has been proposed and tested by Perot & Moin[23]. We use this model to motivate the near boundary terms. The resulting dissipation terms are,

$$\varepsilon_\phi = [2\alpha\tfrac{\varepsilon}{k}\beta + 2\nu(\nabla\phi^{1/2}\cdot\nabla\phi^{1/2})/\phi]\phi \qquad (6a)$$

$$\varepsilon_\phi = [\alpha\tfrac{\varepsilon}{k}\beta + 2\nu(\nabla k^{1/2}\cdot\nabla\phi^{1/2})/(k\phi)^{1/2}]\psi \qquad (6b)$$

where $\beta = \left(\frac{1+CwT2*rr\cdot rr/\mathrm{Re}}{1+CwtT1/\mathrm{Re}}\right)^{1/2}$, $rr = 1.5\phi/k$, and $\mathrm{Re} = k^2/(\nu\varepsilon)$. The gradient terms make the model exact at walls and free surfaces. The parameter β turns the standard part of the model off at very low Reynolds numbers. Both these modifications are significant only well within the laminar sublayer but can not be neglected when walls or surfaces are present.

The model would be more elegant without the inclusion of β, but this does not seem possible for a model that integrates the equations up to the wall. All low Reynolds number models damp the dissipation term near the wall. The fundamental problem appears to be that ε/k is not the correct inverse time scale in highly anisotropic regions such as near a wall or surface. The current form for β is *ad hoc* and is essentially borrowed from Parneix, Laurence & Durbin[24]. However, the exact form is not important, and we have not investigated simpler alternatives at this time. Note that the only model constants which enter the dissipation model appear in the parameter β, which is effective only very close to a wall or surface.

3.2 Pressure Coupling

Coupling between the pressure gradient and velocity is one of the important physical effects that can be captured by Reynolds stress transport models. This correlation produces counter-gradient transport (a reduction of the turbulent transport term), as well as a redistribution of turbulent energy among the various Reynolds stress components. The development of the pressure coupling terms is motivated by the exact evolution equation for the Reynolds stress anisotropy tensor, $\mathbf{a} = (\mathbf{R} - \frac{2}{3}k\mathbf{I})/k$. This evolution equation contains the pressure coupling term as one of the source terms. The model assumes that the pressure coupling term is proportional to the other source terms in the anisotropy evolution equation. This assumption gives, $\Pi = Cp1(\varepsilon - \frac{\varepsilon}{k}\mathbf{R}) - Cp2\,(\mathbf{P} - \frac{P}{k}\mathbf{R})$, where Π is the pressure coupling term, $\mathbf{P}$ is the Reynolds stress production tensor, and P is the production of turbulent kinetic energy.

When the previously proposed dissipation model is introduced into this equation (without the near wall corrections) the pressure coupling term becomes, $\Pi = Cp1(1-\alpha)\frac{\varepsilon}{k}(\frac{2}{3}k\mathbf{I} - \mathbf{R}) - Cp2\,(\mathbf{P} - \frac{P}{k}\mathbf{R})$. This bears considerable resemblance to classic pressure coupling models. The second term is similar to the Isotropization of Production (IP) model of Launder, Reece & Rodi[10] (which is $Cp2(\mathbf{P} - \frac{2}{3}P\mathbf{I})$). To obtain the correct initial behavior of the shear-stress in rapidly distorted homogeneous shear flows a value of $Cp2 = 3/5$ is required.

The first term is a return-to-isotropy term multiplied by (1-α). In isotropic turbulence (1-α) = ½, and near walls and surfaces (1-α) = 0. This is in qualitative agreement with the simulations of Perot & Moin[25] and predictions of Lumley[11] which indicate that return-to-isotropy is a good approximation for nearly isotropic turbulence and is not present at low Reynolds numbers and near boundaries. The value of the 'Rotta constant' for the classic return to isotropy model is commonly taken in the range 1.5 to almost 3.0. The value of $Cp1 = 4.2$ used in this work gives an equivalent Rotta constant of 1.6 for shear flows and 2.1 for isotropic turbulence. In order to obtain no return-to-isotropy effect at low turbulent Reynolds numbers the return-to-isotropy term is divided by $(1 + 25/\mathrm{Re})$ where Re is the turbulent Reynolds number. This near wall modification is similar to the near wall modification of the dissipation model and it too only comes into effect in the laminar sublayer. Its actual form (or the value of 25) is not particularly critical to the model.

This basic pressure coupling model (as well as its more classic variations) produces too much production of the turbulent potentials in the near wall region. Durbin[26] approached the problem of too much production near the wall by using an additional elliptic equation to damp the pressure coupling term near the wall. This has the added benefit of allowing the imposition of an additional boundary condition that could then be used to force the correct asymptotic behavior of the potentials. This is an elegant solution but was not found necessary in this modeling framework. Interestingly, the same effect can be obtained with the following near wall pressure coupling term, $-\frac{1}{\alpha}\frac{1}{(1+Cp3\nu_T/\nu]}\varepsilon$. This term has the correct asymptotic behavior near both walls and free-surfaces, and disappears at high Reynolds numbers. Direct numerical simulations of Perot & Moin[27] indicate that the pressure coupling term is strongly influenced by viscous dissipation near walls and surfaces. A value of $Cp3 = 0.12$ is used in the subsequent calculations.

The final enhancement to the pressure coupling term is formulated to allow the scalar potential to obtain the correct behavior for rapidly distorted shear flow. The scalar potential has the interesting property that it decreases when the flow is suddenly sheared. For this reason we add the following term, $(Cp2 + Cp4)(\frac{\psi\cdot\psi}{\nu_T}\frac{1}{(1+25/\mathrm{Re})} - P)(2\alpha\mathbf{R}/k)$. The constant is set by Rapid Distortion Theory (RDT) to be $Cp4 = 6/7$. When the eddy viscosity hypothesis is an accurate approximation this term is small or zero. It only becomes significant when the flow is in a strong non-equilibrium situation (such as RDT). If one assumes that Cp2 and Cp4 must be set to obtain the correct RDT response, then the only free constants in the modeling of pressure coupling term are Cp1 and the near-wall/low Re corrections.

3.3 Turbulent Transport

The enhanced transport which turbulence invariably produces is modeled using a gradient transport hypothesis. This results in the following source terms for the scalar and vector potentials, $\nabla\cdot(\nu_T/\sigma_k)\nabla\phi$ and $\nabla\cdot(\nu_T/\sigma_k)\nabla\psi$. In flows with a single inhomogeneous direction these models are equivalent to the Daly & Harlow[12] model for Reynolds stress turbulent transport, where the eddy viscosity is defined as $\nu_T = C_\mu\frac{\phi k}{\varepsilon}$, with $C_\mu = .21$. The constant, $\sigma_k = 0.79$, is the same for both the potentials and the turbulent kinetic energy transport term. It was obtained by solving the *k* equation in turbulent channel flow, using the exact production and dissipation (from DNS data), and obtaining a best fit. Note that this is somewhat lower than the conventional value of 1.0. However, the conventional value is set so as to counteract some inadequacies of the ε equation and the current value agrees well with other DNS simulations[28]. The value of $\sigma_k = 0.79$ gives an equivalent Daly & Harlow constant which is well within the range [.20 to .25] commonly used for that model.

3.4 Rotation

The principal effects of system rotation appear explicitly in the Reynolds stress transport equations via the term, $2(\Omega\times\mathbf{R} + [\Omega\times\mathbf{R}]^T)$, where Ω is the system rotation vector. The trace of this term is zero so rotation has no explicit effect on the turbulent kinetic energy. This is one reason why the *k*/ε model and its variants often represent rotation effects fairly poorly. For a constant (in space) rotation rate, the corresponding scalar potential source term is $-4\Omega\cdot\psi$. For fully three-dimensional flows the vector potential rotation term is complex and is given by, $2\Omega\phi + \nabla^{-2}\{2\Omega\cdot[\nabla(\mathbf{f}) + \nabla\times(\nabla\times\mathbf{R})^T]\}$ where **f** is the turbulent body force. For a two-dimensional flow the term involving **f** is zero. The last term must be modeled in any dimension since the full Reynolds stress tensor is no longer calculated. Assuming that the Reynolds stress tensor is isotropic and the flow is 2D gives $-2\Omega(\frac{2}{3}k - \phi)$ for the vector potential rotation term. Both rotation terms have the important property of breaking system symmetries under the influence of rotation. Besides introducing an addition explicit

production term rotation has secondary effects on the turbulence evolution. These secondary effects have not been included in the model at this time.

3.5 Transition

Transition is a complex phenomenon that is dependent both on the flow configuration and initial disturbance spectrum. Many low Reynolds number two equations models have been shown to be able to predict at least the qualitative behavior of relaminarization and bypass transition[29-31]. Predictions of transition using Reynolds stress transport models have had less success[32]. In this model we introduce a term which allows transition to be controlled, but which does not otherwise influence the turbulence predictions. The following term is included in the scalar potential equation, $C_t P(1-\frac{1.5\phi}{k})$. C_t can be taken anywhere in the range 0.01 to 1.0e-5. The smaller values delay the transition process and increase the transition time by an order of magnitude. The ability to tune this constant gives the model considerable flexibility in predicting different types of transition processes.

3.6 Turbulent Kinetic Energy and Dissipation Equations

The turbulent potential transport equations are supplemented by transport equations for the turbulent kinetic energy and the dissipation. These equations where chosen because they are widely used for engineering solutions, and because data for both k and ε are widely available. These equations enable the system to behave correctly in time developing or convection dominated situations, and help to make the equations system more robust in situations where the mean flow gradients are small.

If computational time is a serious issue, algebraic models for either or both of these variables can be used. In particular, for shear dominated flows, $k=\frac{3}{2}(\phi+E\psi\cdot\psi/\phi)$ and $\varepsilon = C_\mu P\frac{\phi k}{\psi\cdot\psi}$ are good approximations. The latter expression is equivalent to the linear eddy viscosity hypothesis (though used in a different context). Computations of turbulent channel flow with these algebraic expressions and $E=1.1$ showed a reasonable agreement with the DNS data of Kim, Moin & Moser[33].

The k and ε transport equations used in this study are the standard implementation with a few exceptions. As mentioned previously σ_k has been reduced from 1.0 to 0.79 after careful comparisons with the DNS data of turbulent channel flow. In addition, following the example of Durbin[26], the inverse time scale in the ε equation is modified by β. Finally, an additional transport term has been added to the ε equation to reduce the dissipation in regions of strong turbulent kinetic energy diffusion. It is given by, $C_{\varepsilon 3}(1-\alpha)2\varepsilon\nabla\cdot\frac{\phi}{\varepsilon}\nabla k$ and $C_{\varepsilon 3}=0.17$. This term has the property that it allows both the mixing layer and the boundary layer to be modeled without any adjustments to the other model constants. In addition, the center of turbulent channel flow is represented more accurately when this term is present.

The constants in the k/ε model (specifically $C_{\varepsilon 1}=1.5$ and $C_{\varepsilon 2}=1.83$) determine the growth rate of the turbulence in homogeneous shear flows at long times. The standard k/ε model predicts a growth rate of 0.243. The different definition of the eddy viscosity used in this model leads to a much more accurate growth rate of 0.143, which is very close to experimental measurements[34].

4. Turbulent Body Force Potential Model

4.1 Model Summary

The transport equations that constitute the turbulent potential model are summarized below.

$$\frac{Dk}{Dt} = \nabla \cdot (\nu + \nu_T / \sigma_k)\nabla k + P - \varepsilon$$

$$\frac{D\varepsilon}{Dt} = \nabla \cdot (\nu + \nu_T / \sigma_\varepsilon)\nabla \varepsilon + \beta \frac{\varepsilon}{k}(C_{\varepsilon 1} P - C_{\varepsilon 2}\varepsilon) + C_{\varepsilon 3}(1-\alpha)2\varepsilon \nabla \cdot \tfrac{\phi}{\varepsilon} \nabla k$$

$$\frac{D\phi}{Dt} = \nabla \cdot (\nu + \nu_T / \sigma_k)\nabla \phi - \left(\beta 2\alpha \frac{\varepsilon}{k} + \frac{2\nu(\nabla \phi^{1/2} \cdot \nabla \phi^{1/2})}{\phi} + \frac{\varepsilon}{k} \frac{2}{(1 + Cp3 \frac{\nu_T}{\nu})} \right) \phi$$
$$+ Cp1 \frac{\varepsilon}{k} \frac{(1-\alpha)}{(1 + 25/\mathrm{Re})} (\tfrac{2}{3} k - \phi) + Cp2 \frac{\phi}{k} P - 4\Omega \cdot \psi + C_t (1-\alpha) P$$
$$+ (Cp2 + Cp4) 2\alpha \frac{\phi}{k} \left(\frac{\psi \cdot \psi}{\nu_T (1 + 25/\mathrm{Re})} - P \right)$$

$$\frac{D\psi}{Dt} = \nabla \cdot (\nu + \nu_T / \sigma_k)\nabla \psi - \left(\beta \alpha \frac{\varepsilon}{k} + \frac{2\nu(\nabla k^{1/2} \cdot \nabla \phi^{1/2})}{(k\phi)^{1/2}} + \frac{\varepsilon}{k} \frac{1}{(1 + Cp3 \frac{\nu_T}{\nu})} \right) \psi$$
$$(1 - Cp2)\phi\omega - Cp1 \frac{\varepsilon}{k} \frac{(1-\alpha)}{(1 + 25/\mathrm{Re})} \psi + Cp2 \frac{\psi}{k} P - 4\Omega(\tfrac{2}{3} k - \phi)$$
$$+ (Cp2 + Cp4) 2\alpha \frac{\psi}{k} \left(\frac{\psi \cdot \psi}{\nu_T (1 + 25/\mathrm{Re})} - P \right)$$

where

$$P = \psi \cdot \omega, \quad \nu_T = C_\mu \frac{\phi k}{\varepsilon}, \quad \beta = \left(\tfrac{1 + CwT2^* rr \cdot rr / \mathrm{Re}}{1 + CwT1 / \mathrm{Re}} \right)^{1/2}, \quad \alpha = 1/(1 + 1.5 \tfrac{\phi}{k}), \quad \text{and} \quad \mathrm{Re} = k^2 / (\nu\varepsilon).$$

Initially these equations appear daunting. In fact they represent a fairly simple extension of the classic *k/ε* equation system, and are relatively simple compared to Reynolds stress transport equation models. The second source term in the potential equations (in parentheses) is a dissipation-like term. This term is a standard dissipation model with two near-wall/surface modifications, one for the dissipation and one for the near wall pressure correlation term. These modifications are active in the laminar sublayer and allow the model to obtain the correct asymptotic behavior in the sublayer. The source terms involving the constants Cp1 and Cp2 are pressure-strain redistribution terms. The slow pressure-strain is based on return-to-isotropy and the fast pressure-strain is based on isotropization of the production model. The constants are set to common values for these models. The effect of system rotation has been explicitly included, and the scalar transport equation has a transition term involving the constant C_t. The transition term does not effect model results for fully developed turbulence, but does allow control of transition to turbulence.

5. Potential Model Predictions

In this section the predictions of the turbulent potential model are presented for a number of different turbulent flows. These predictions are compared to experimental or direct numerical simulation data, and other RANS turbulence models whenever possible. Results will be presented for channel flow at two different Reynolds numbers, rotating channel flow at moderate rotation rates, a mixing layer, two adverse pressure gradient boundary layers, and preliminary results of turbulent flow over a backward facing step. In addition, the ability to control the transition rate in channel flow will be demonstrated.

5.1 Channel Flow

The geometric simplicity of turbulent channel flow makes it a very attractive candidate for the testing of turbulence models. Due to the fact that the convective derivative is identically zero in this flow (and the viscous term is small everywhere but close to the wall), this flow is very sensitive to the modeled source terms and is a reasonably difficult test case of a turbulence model. This is particularly true if the model does not use 'law of the wall' boundary conditions and integrates up to the wall.

Most low Reynolds number models which are capable of integrating to the wall, use an abundance of damping functions and other near wall modifications to capture the near wall region. Functions of the wall normal vector or wall normal distance are poorly defined in complex geometries. Damping functions that use the turbulent Reynolds are more general, but can also lead to instability in low turbulence regions far from walls and must be implemented carefully.

The channel flow calculations presented in Figure 1 demonstrate the potential model's ability to represent near wall behavior without the use of damping functions. This figure shows the mean velocity ($\times 10^{-1}$), turbulent kinetic energy, dissipation rate ($\times 10^{-1}$), normal Reynolds stress (R_{22}) and shear stress (R_{12}) in one half of the symmetric channel. The Reynolds number based on the mean velocity and channel half width is 7900 and the pressure gradient is equal to 1.0. The Reynolds number based on the shear velocity (u^*) is 395. The DNS data of Kim [35] is given by the dashed lines, and solid lines indicate the model predictions.

Note that these calculations were performed with a fixed pressure gradient not a fixed mass flux, and therefore the mean velocity predictions are much more sensitive to the model (a fixed mass essentially renormalizes the velocity profile so that the integral is always correct). Nevertheless, the agreement with the DNS data is extremely good. In part, this good agreement is a result of the fact that some of the near-wall model constants were tuned using this flow. However, the model is not particularly sensitive to these constants, and the good predictions for all the turbulence quantities suggests that the agreement is due to more than just model tuning.

A reasonable criticism of model comparisons with DNS data is that the Reynolds numbers are fairly low. (The attraction of DNS data is that all turbulence quantities are usually available). A test of the model at higher Reynolds numbers is shown in Figure 2. This figure shows the mean velocity ($\times 10^{-1}$), turbulent kinetic energy, and normal Reynolds stress in one half of the symmetric channel. The Reynolds number based on the mean velocity and channel half width is over ten times higher than the previous figure, 90660, and the pressure gradient is equal to 1.0. The Reynolds number based on the shear velocity (u^*) is 3951. The Large-eddy simulation data of Kravchencko & Moin[36] is given by the dashed lines, and solid lines indicate the model predictions.

At the low end of the Reynolds number spectrum, experiments indicate that turbulent channel flow can not be sustained at Reynolds numbers below about 2000. Viscosity causes the turbulence to dissipate and the flow relaminarizes. The potential model predicts relaminarization at a Reynolds number of 2100 (or 125 based on u^*). The ability of the model to correctly predict relaminarization could be closely related to its ability to predict laminar to turbulent transition.

5.2 Rotating Channel Flow

Rotation is an integral part of many engineering applications (propellers, turbines, pumps, etc) and can not be ignored when developing a general turbulence model. As mentioned previously, rotation has complex effects on turbulence. Rotation produces a Coriolis force which, like the pressure gradient force, can couple with the turbulence and influence its

evolution. The coupling of the Coriolis force with the Reynolds stresses is explicitly captured in Reynolds stress transport equations models, and can be reasonably well approximated by the turbulent potential model. However, there are additional secondary effects due to rotation. At a first level of approximation turbulent eddies act like gyroscopes with individual angular momentum. When rotation is imposed turbulent eddies precess to try and maintain their angular momentum. This precession randomizes the eddy orientations and alters conventional turbulence structures leading to a reduction of the turbulent dissipation rate, and an increased return to isotropy rate.

The scope of this initial work has not allowed for the implementation of models for secondary rotation effects. Nevertheless the potential model does show the correct qualitative features due to system rotation. Figure 3 shows model predictions for rotating channel flow. The Reynolds number is 7900, and the Rossby number ($Ro = \Omega L / U_{\max}$) is equal to 0.07. The entire channel is now displayed since the flow is no longer symmetric about the centerline. The model correctly predicts the qualitative effects of stabilization on the upper wall and enhanced turbulence production on the lower wall. Comparison with experiments[37] indicate that the model prediction is over stabilized on the upper wall. Both the secondary rotation effects described earlier (reduced dissipation and increased return to isotropy) would counteract this tendency of the model.

5.3 Mixing Layer

The mixing layer demonstrates the performance of the potential model for free shear layers. The mixing layer was chosen because it is generally more difficult to predict than jets and wakes. The mixing layer that was calculated involves two parallel streams, the upper stream moving at a speed twice that of the lower stream. The Reynolds number at the downstream location where the profiles are presented is on the order of 10^6 based on the velocity difference and the downstream distance (or roughly 10^5 based on the mixing layer thickness). Figure 4a shows the mean velocity profile, and Figure 4b shows the kinetic energy distribution. The figures are normalized with respect to the mean velocity difference and the mixing layer vorticity thickness (defined by $\delta = (U_2 - U_1) / |\omega_{\max}|$). Symbols indicate the experimental data of Plesniak & Johnston[38]. Dash-dotted lines are the predictions of a standard k/ε model using the boundary layer approximation. Dotted lines are the predictions of the potential model using the boundary layer approximation, and solid lines are the predictions of the potential model using a Navier-Stokes code.

The edges of the experimental data of Plesniak & Johnston display the presence of high levels of free-stream turbulence. Similar DNS simulations[39] suggest that the turbulent kinetic energy falls off more rapidly at the edges when free-stream turbulence is not present. In those experiments the turbulence is essentially zero by $y/\delta = 1.1$. In any case, the k/ε model predicts an abrupt edge to the mixing layer at about half that distance. The tendency for the k/ε model and other models to form sharp fronts is well documented and is a result of the nonlinear nature of the turbulent transport term[40,41]. The boundary layer solution of the potential model shows smoother behavior at the edges, and an improved kinetic energy distribution. Full solutions using the turbulent potential model show even better agreement with the experimental data, and a behavior at the mixing layer edge that is close to the DNS simulations of Rogers & Moser[39].

The strong asymmetry of the modeled turbulent kinetic energy profile versus the experimental data is probably a result of the scaling of the experimental data. The experiments were actually performed in a configuration where the two fluid streams had velocities that were close in magnitude. The data were then scaled on the velocity difference. While the physics of the mixing layer core is dominated by the velocity difference, the decay of turbulence at the layer edges is a strong function of the actual velocity magnitude.

Experiments and DNS simulations indicate that the nondimensional peak value of the normal Reynolds stress (R_{22}) should be in the range 0.016 to 0.0017, and the peak value of the shear stress (R_{12}) should be in the range -0.010 to -0.0011. The potential model predicts a peak value of 0.015 for the normal Reynolds stress and –0.0012 for the peak shear stress. Plesniak et al. reported a spreading rate ($\frac{d\delta}{dx}$) of 0.061, but experiments vary from 0.054 to 0.065. k/ε models typically under predict the spreading rate by about 15% and produce spreading rates of about 0.052. The spreading rate predicted by the potential model is 0.063, which is in close agreement with experimental norms.

5.4 Adverse Pressure-Gradient Boundary Layer

Adverse pressure-gradient boundary layers represent a situation where the classic assumptions of turbulence modeling are not well approximated. In particular, the turbulence is not in equilibrium with the mean flow, and the eddy viscosity hypothesis is a poor approximation. Two equation models (even the more elegant models, such as Durbin's elliptic relation model) sometimes have problems predicting adverse pressure boundary layers[26]. However, models which predict the shear stress directly (Johnson & King, and Bradshaw, Ferriss & Atwell, and full Reynolds stress closures) generally show considerable success with these types of flows. Since the potential model also directly predicts a quantity akin to the shear stress, it is expected to perform well in these situations.

A common adverse pressure-gradient flow for tests of turbulence models is the experiment of Samuel & Joubert[42]. The friction coefficient as a function of the downstream distance for this flow is shown in Figure 5. Circles indicate the experimental data and the solid line shows the model prediction. In addition, the experimental and computed velocity profiles at two downstream locations (Samuel & Joubert's station 9 and station 12) are shown in Figure 6. The agreement is very satisfactory.

A more difficult test of the model's ability to capture separating flows is given by the experiments of Schubauer & Spangenberg[43]. This experiment has a very strong adverse pressure-gradient and presents data very close to the separation point. Figure 7 shows velocity profiles for three downstream locations of this flow compared with the experiments. The agreement continues to be reasonable.

5.5 Backward Facing Step

The backward facing step displays a number of complex interacting flow phenomena, such as a detached shear layer, boundary layers, reattachment, recirculation, and boundary layer recovery. Two-equation models which use wall functions have had some success predicting this flow, but models which integrate up to the wall have more difficulty since the damping functions are usually ill-defined at the corners and often unstable at the reattachment point. Those models which do predict the reattachment point of the backstep correctly, tend to under predict the recovery of the boundary layer at higher Reynolds numbers.

The computed streamlines for the backward facing step at a Reynolds number of 5100 (based on the step height, h) and an expansion ratio of 1.2 are shown in Figure 8. This geometry corresponds to the DNS simulations of Le & Moin[44] and the experimental results of Jovic & Driver[45]. The step is located at y/h=1 and x/h=0. The calculation domain extends from –3h upstream of the step to 27h downstream and 6h in the vertical direction. The mesh consisted of 120x120 quadrilateral cells stretched so as to resolve the boundary layers, shear layer, and the reattachment zone. The computed reattachment point was found to be 6.36 step-heights downstream of the step. This corresponds very favorably with the value of 6.28h found by the DNS simulations and 6.1h found by the experiments. A standard k/e formulation typically predicts premature reattachment at around 5.4h, though enhanced models predict the reattachment point correctly.

DNS data and model predictions for the mean velocity are shown for a number of downstream positions in Figure 9. Squares indicate the DNS results and solid lines indicate the model predictions. The magnitude of the velocity in the recirculation bubble is slightly under predicted, but the overall agreement is very reasonable for this initial formulation of the model.

5.6 Transition

The ability to predict transition is an important component of many engineering problems. However, transition is usually an afterthought in the development of turbulence models. It may be impossible to accurately predict all the different types of transition with a single RANS model. In this work, a pragmatic approach is taken, where the user is able to control the transition development. It is hypothesized that this approach will allow fairly broad classes of transition problems (such as natural transition in boundary layers, or bypass transition in mixing layers) to be calculated using a single parameter value and without explicit user intervention (such as tripping).

A demonstration of natural transition control has been performed for transition in the channel flow. The mean velocity is initially uniform and set to a value of 10. The initial turbulent kinetic energy is 0.01% and the initial eddy viscosity is equal to 0.1ν. The channel Reynolds number based on the channel half height is 3300. Figure 10 shows the development of the maximum turbulent kinetic energy as a function of time for various values of the transition constant C_t. The model correctly shows exponential growth of the turbulent kinetic energy during the transition process, with the rate of growth controlled by the transition constant. The other turbulence quantities behave similarly. If the viscosity is increased significantly so that the channel Reynolds number is 1600, then the flow does not transition even for values of C_t as high as 0.001.

Most RANS turbulence models that display transition-like behavior require relatively high levels of free-stream turbulence to trigger the transition event (essentially by-pass transition). Usually, the transition time is dictated by how long it takes the free-stream turbulence to diffuse into the boundary layer and is difficult to control. The potential model does not rely on free-stream turbulence to trigger transition. This means that it can predict transition when the free-stream turbulence is very small, and more importantly, that the transition behavior can be explicitly controlled.

6. Conclusion

A new approach to RANS turbulence modeling has been presented based on the scalar and vector potentials of the turbulent body force vector – the divergence of the Reynolds stress tensor. This approach lies somewhere between two-equation models and full Reynolds stress transport equations models. It shares with Reynolds stress transport equation models the ability to accurately predict strongly non-equilibrium flows, but it has a cost and complexity comparable to enhanced two-equation models.

Analysis of the 'turbulent potentials' indicates that they are not just mathematical constructs, but physically relevant turbulence quantities closely related to the Reynolds stresses. The scalar potential can be thought of as a 'turbulent pressure', and is a valuable indicator of turbulence anisotropy. The vector potential can be thought of as a 'turbulent vorticity'. In fact the linear eddy-viscosity hypothesis is equivalent to the expression $\psi = \nu_T \omega$ if second derivatives of the eddy viscosity are assumed to be small. Like the vorticity, only one component of the vector potential is non-zero in two-dimensional and axisymmetric mean flows.

Transport equations for the turbulent potentials have been derived, and models for the source terms in those equations were proposed based largely on methods and models developed for the Reynolds stress transport equations. The formulation has been demonstrated to be computationally tractable, and robust convergence to steady-state was achieved for all the test cases even though all the transport equations were uncoupled numerically. The proposed transport equations can be integrated up to a wall or surface; they do not require wall functions. In addition, no functions of the wall normal coordinate have been used, so the model can be implemented easily into existing flow solvers and complex geometries.

The channel flow simulations showed good agreement with DNS data at both high and low Reynolds numbers. Relaminarization was predicted correctly, and the ability to transition to full turbulence from very small free-stream turbulence levels ('natural transition') was demonstrated. In addition, the model was shown to have the ability to control the transition rate and transition point. Simulations of rotating channel flow showed the models ability to capture the qualitative effects of rotation, namely enhanced production on the unstable side, and turbulence suppression on the stable side. However, additional modification are necessary to capture secondary rotation effects and obtain good quantitative agreement.

Calculations of a developing mixing layer captured the mean velocity and kinetic energy profiles well. The mixing layer edge was better resolved than standard two equation models. The simulation of two adverse pressure gradient boundary layers gave the correct boundary layer growth and velocity profiles as separation was approached. Simulations of a backward facing step captured the reattachment length correctly and produced reasonable agreement with DNS data for the mean velocity. However, the behavior of the turbulence in the attachment zone could be improved. It seems likely that the model requires additional terms that appear only when the flow has more than one inhomogeneous direction.

Acknowledgments

This work was performed while the author was employed by Aquasions Inc. and was funded, in part, by NASA-Ames Research Center in the form of a Phase I SBIR Grant. Their support is gratefully acknowledged. The author is also greatly indebted to Parviz Moin for his encouragement and support and to Paul Durbin and Sanjiva Lele for their many insightful comments.

References

[1]W. Rodi, "A new algebraic relation for calculating the Reynolds stresses", ZAMM **56**, 219-221 (1976).

[2]S. B. Pope, "A more general effective-viscosity hypothesis", J. Fluid Mech. **72**, 331-340 (1975).

[3]T. B. Gatski & C. G. Speziale, "On explicit algebraic stress models for complex turbulent flows", J. Fluid Mech. **254**, 59-78 (1993).

[4]T. J. Craft, B. E. Launder & K. Suga, "Extending the applicability of eddy viscosity models through the use of deformation invarients and non-linear elements" Proc. 5th Int. Symp. On Refined Flow Modelling and Turbulence Measurements, 125-132, Presses Ponts et Chaussees, Paris.

[5]T. S. Lund & E. A. Novikov, "Parameterization of subgrid-scale stress by the velocity gradient tensor", Ann. Res. Briefs, Center for Turbulence Research (Stanford University/ NASA Ames), 27-43 (1992).

[6]D. A. Johnson & L. S. King, "A mathematically simple turbulence closure model for attached and seperated turbulent boundary layers", AIAA Journal, **23** (11), 1684-1692 (1985)

[7]P. Bradshaw, D. H. Ferriss & N. P. Atwell, "Calculations of boundary-layer development using the turbulent energy equation", J. Fluid Mech. **28**, 593-616 (1967).

[8]S. J. Kline, M. V. Cockrell, M. V. Morkovin & G. Sovan, eds. *Computation of Turbulent Boundary-Layers*, Vol I, AFOSR-IFP-Stanford Conference. (1968).

[9]J. Rotta, "Statistische Theorie nichthomogener Turbulenz I", Z. für Physik **129**, 547-572 (1951).

[10]B. E. Launder, G. J. Reece & W. Rodi, "Progress in the development of a Reynolds-stress turbulence closure", J. Fluid Mech. **68**, 537-566 (1975).

[11]J. L. Lumley, "The mathematical modelling of turbulent flows", Applied Mathematical Modelling, **10**, 190 (1978).

[12]B. J. Daly, & F. H. Harlow, "Transport equations in turbulence". Phys. Fluids **13**, 2634-2649 (1970).

[13]J. B Perot & P. Moin, "A new approach to turbulence modeling", Proceedings of the 1996 Summer Program, Center for Turbulence Research (Stanford University/ NASA Ames), 35-46, (1996).

[14]J. Wu, Y. Zhou & J. Wu, "Reduced stress tensor and dissipation and the transport of the Lamb vector", ICASE Report No 96-2, (1996)

[15]H. Marmanis, "Analogy between the Navier-Stokes equations and Maxwell's equations: applications to turbulence", Phys. Fluids **10** (6), 1428-1437 (1998)

[16]S. G. Saddoughi, "Local isotropy in strained turbulent boundary layers at high Reynolds number", Ann. Res. Briefs, Center for Turbulence Research (Stanford University/ NASA Ames), 347-364 (1993).

[17]M. Hallbäck, J. Groth & A. V. Johansson, "An algebraic model for non-isotropic turbulent dissipation rate in Reynolds stress closures", Phys. Fluids A **3**, 2276-2277 (1990).

[18]P. A. Durbin & C. G. Speziale, "Local anisotropy in strained turbulence at high Reynolds numbers", ASME J. Fluids Eng., **113**, 707-709, (1991).

[19]N. N. Mansour, J. Kim & P. Moin, "Reynolds-stress and dissipation-rate budgets in a turbulent channel flow", J. Fluid Mech. **194**, 15-44 (1988).

[20]K. Hanjalic & B. E. Launder, "Contribution towards a Reynolds-stress turbulence closure for low-Reynolds-number turbulence", J. Fluid Mech. **74**, 593-610 (1976).

[21]T. J. Craft & B. E. Launder, "Improvements in Reynolds-stress modelling for complex flow geometries", Proc. 10th Symposium on Turbulent Shear Flows, Penn State University (1995).

[22]M. Hallbäck, "Development of Reynolds stress closures of homogeneous turbulence through physical and numerical experiments." Doctoral Thesis, Royal Institute of Technology, Sweden. (1993)

[23]J. B. Perot & P. Moin, "A near-wall model for the dissipation tensor", Proceedings of the 11th Australasian Fluid Mechanics Conference, University of Tasmania, Hobart, 471-474 (1992)

[24]S. Parneix, , D. Laurence, & P. A Durbin, "Second moment closure analysis of the backstep flow database", Proc. of the 1996 Summer Program, Center for Turbulence Research (Stanford University/ NASA Ames), 47-62 (1996).

[25]J. B. Perot & P. Moin, "Shear-free turbulent boundary layers. Part 1. Physical insights into near-wall turbulence", J. Fluid Mech. **295**, 199-227 (1995)

[26]P. A. Durbin, "A Reynolds stress model for near-wall turbulence", J. Fluid Mech. **249**, 465-498 (1993).

[27]J. B. Perot & P. Moin, "Shear-free turbulent boundary layers. Part 2. New concepts for Reynolds stress transport equation modeling of inhomogeneous flows", J. Fluid Mech. **295**, 229-245 (1995).

[28]J. B. Cazalbou & P. Bradshaw, "Turbulent transport in wall-bounded flows. Evaluation of model coefficients using direct numerical simulation", Phys. Fluids **5** (12), 3233-3239 (1993).

[29]S. L. Liu, "The prediction of boundary layer transition using low Reynolds number k-ε turbulence model", Proc. 4th Asian Congress of Fluid Mechanics, Hong Kong, Vol 1, A9. (1989)

[30]E. Arad, M. Berger & M. Wolfshtein, "Numerical calculations of transitional boundary layers", Int. J. Num. Methods Fluids **2**, 1-23 (1982).

[31]W. Rodi & G. Scheuerer, "Calculation of laminar-turbulent boundary layer transition on turbine blades", AGARD CP 390 18-1 (1984).

[32]A. M. Savill, "One-point closure applied to transition", T*urbulence and Transition Modelling*, Hallbäck, Henningson, Johansson & Alfredson, eds. Kluwer Academic Publishers, Boston. 233-268 (1996).

[33]J. Kim, P. Moin & R. Moser, "Turbulence statistics in fully developed channel flow at low Reynolds number", J. Fluid Mech. **177**, 133-166 (1987).

[34]S. Tavoularis & S. Corrsin, "Experiments in nearly homogeneous turbulent shear flows with a uniform mean temperature gradient, Part I.", J. Fluid Mech. **104**, 311-347 (1981).

[35]J. Kim, private communication, (1996).

[36]A. G Kravchenko, P. Moin & R. Moser, "Zonal embedded grids for numerical simulation of wall-bounded turbulent flows", J. Comput. Phys. **127**, 412-423 (1996).

[37]P. Johnston, R. M. Halleen & D. K. Lezius, "Effects of spanwise rotation on the strucure of two-dimensional fully developed channel flow", J. Fluid Mech. **56** (3), 533-557 (1992).

[38]M. W. Plesniak & J. P. Johnston, "The effects of longitudinal curvature on turbulent two-stream mixing layers". Report No. MD-54, Dept. of Mech. Eng., Stanford University. (1989)

[39]M. M. Rogers, & R. D. Moser, "Direct simulation of a self-similar turbulent mixing layer", Phys. Fluids **6** (2), 903-920 (1994).

[40]F. R. Menter, "Influence of freestream values on k-ω turbulence model predictions", AIAA Journal, **30** (6), 1657-1661 (1992).

[41]P. R. Spalart & S. R. Allmaras, "A one-equation turbulence model for aerodynamic flows", AIAA-92-0439 (1992)

[42]A. E. Samuel & P. N. Joubert, "A boundary layer developing in an increasingly adverse pressure gradient", J. Fluid Mech. **66**, 481-505 (1974).

[43]G. B. Schubauer & W. G. Spangenberg, , "Flow A (4400)", *Computation of Turbulent Boundary Layers, Volume II – Compiled Data*., D. E. Coles & E. A. Hirst, eds. , 416 (1968).

[44]H. Le, P. Moin & J. Kim, "Direct numerical simulation of turbulent flow over a backward-facing step", J. Fluid Mech. **330**, 349-374 (1997).

[45]S. Jovic & D. M. Driver, "Reynolds number effects on the skin friction in separated flows behind a backward facing step," Experiments in Fluids **18**, 464-467 (1995).

Figure 1. *Model predictions of turbulent channel flow at a Reynolds number of 7900 compared with the direct numerical simulation data of Kim.*

Figure 2. *Model predictions of turbulent channel flow at a Reynolds number of 90,660 compared with the Large-eddy simulation data of Kravchenko & Moin. Dashed lines are the LES calculations and solid lines are the model predictions.*

Figure 3. *Model predictions of rotating channel flow at a Reynolds number of 7900 and Rossby number of 0.07.*

Figure 4. *Model predictions of a high Reynolds number turbulent mixing layer. (a) mean velocity profile, and (b) turbulent kinetic energy distribution.*

Figure 5. *Friction Coefficent versus downstream distance for the adverse pressure-gradient boundary layer of Samuel & Joubert. Circles are experimental data, and the solid line indicates the turbulent potential model prediction.*

Figure 6. *Experimental (symbols) and calculated (lines) velocity profiles at station 9 and station 12 of the Samuel & Joubert adverse pressure gradient boundary layer.*

Figure 7. *Experimental (symbols) and calculated (lines) velocity profiles for the adverse pressure gradient boundary layer of Schubauer & Spangenberg.*

Figure 8. *Computed streamlines for a backward facing step with a Reynolds number of 5100 and expansion ratio of 1.2.*

Figure 9. *Mean velocity profiles downstream of a backward facing step at a Reynolds number of 5100. Symbols are the DNS data of Le, Moin & Kim. Solid lines are the model predictions.*

Figure 10. *Transition of a uniform channel flow for different values of the transition constant.*

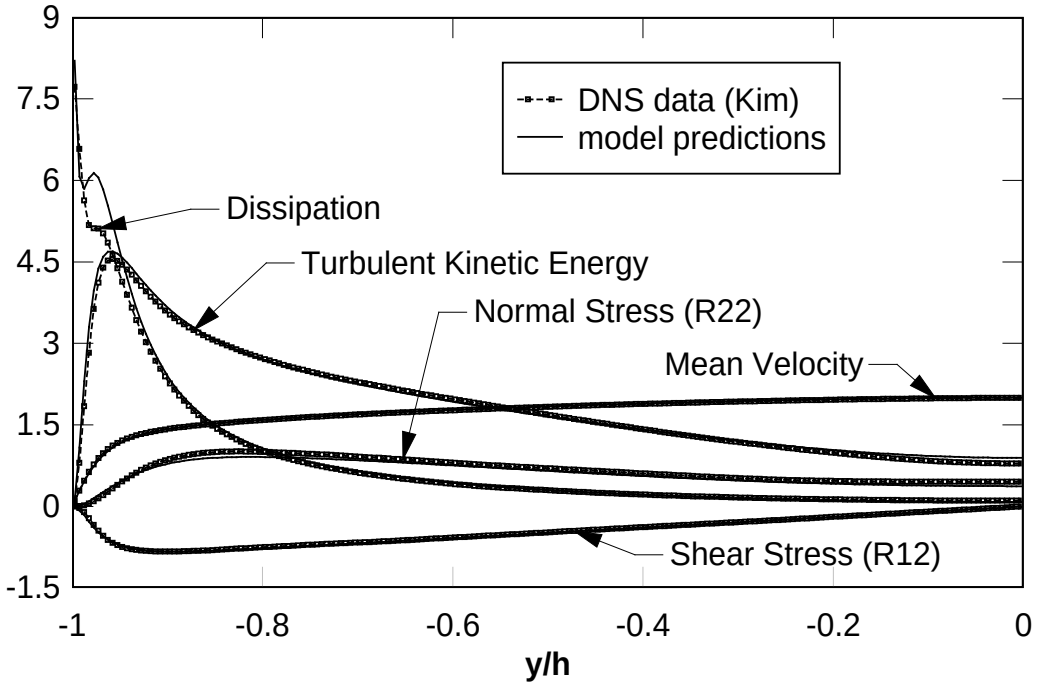

Figure 1: Perot ; Physics of Fluids

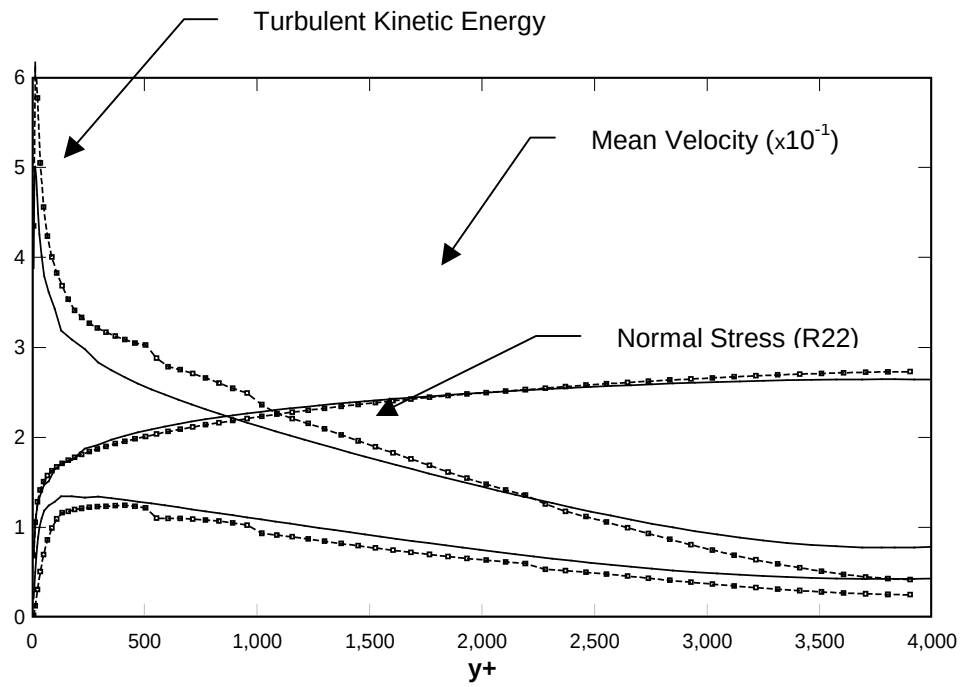

Figure 2: Perot ; Physics of Fluids

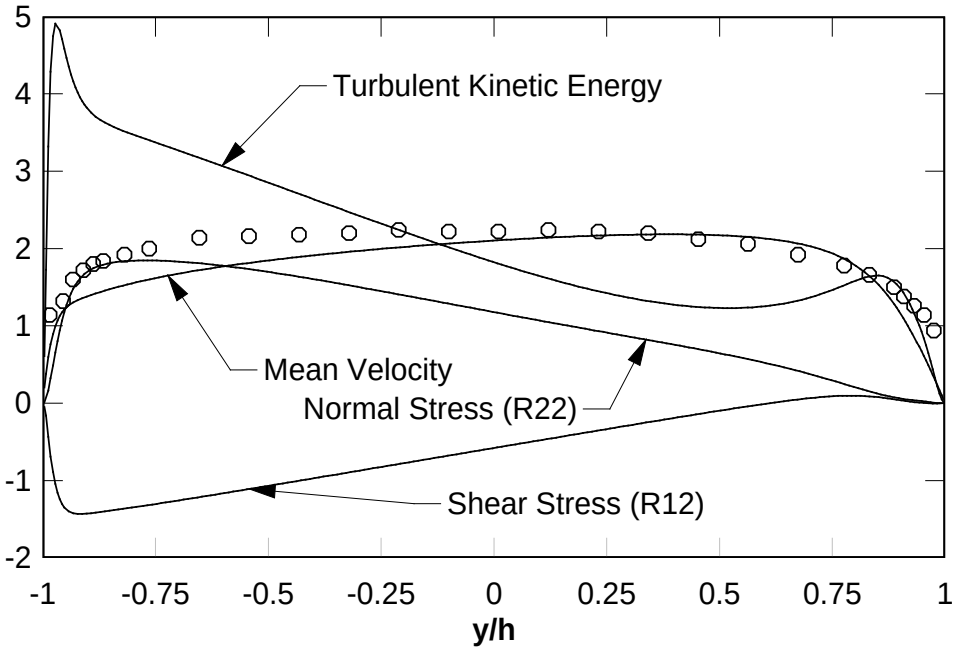

Figure 3: Perot ; Physics of Fluids

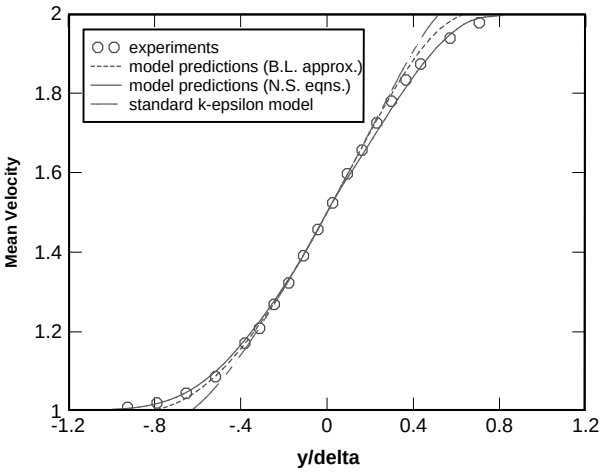

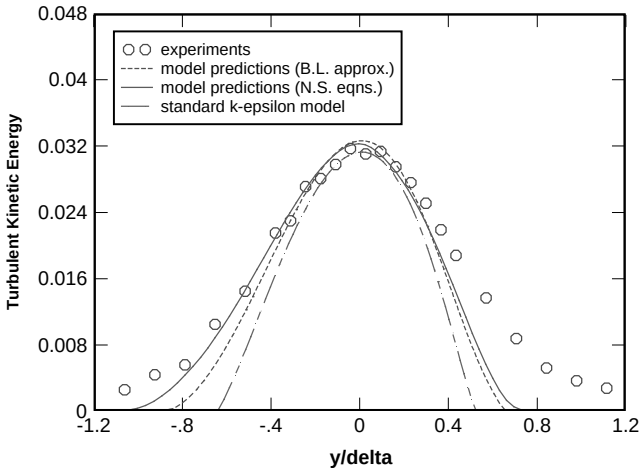

Figure 4: Perot : Physics of Fluids

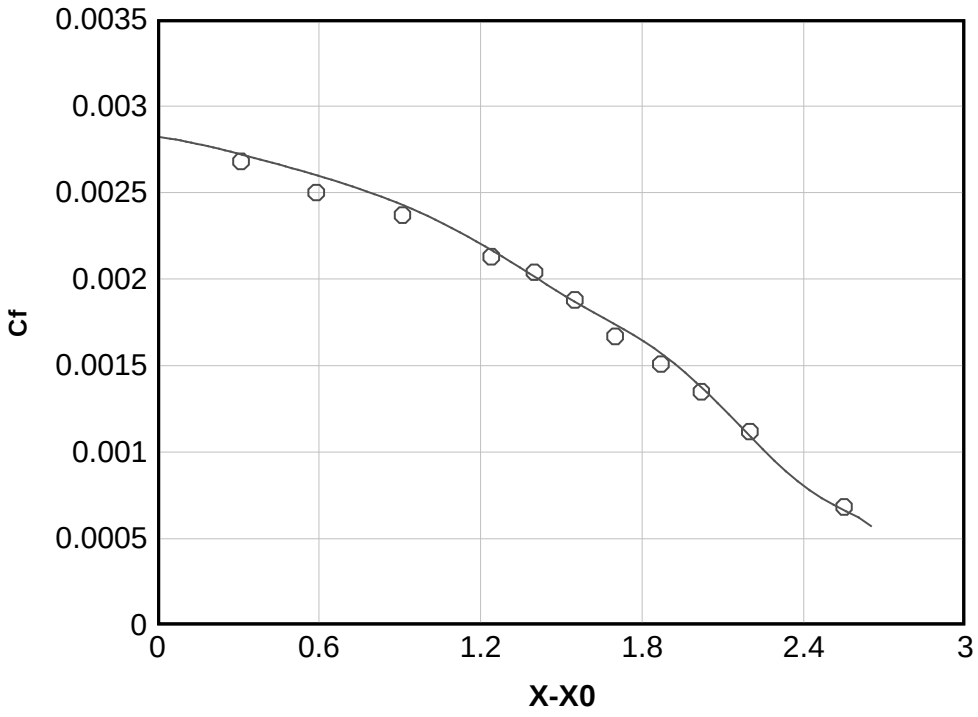

Figure 5: Perot ; Physics of Fluids

Figure 6: Perot ; Physics of Fluids

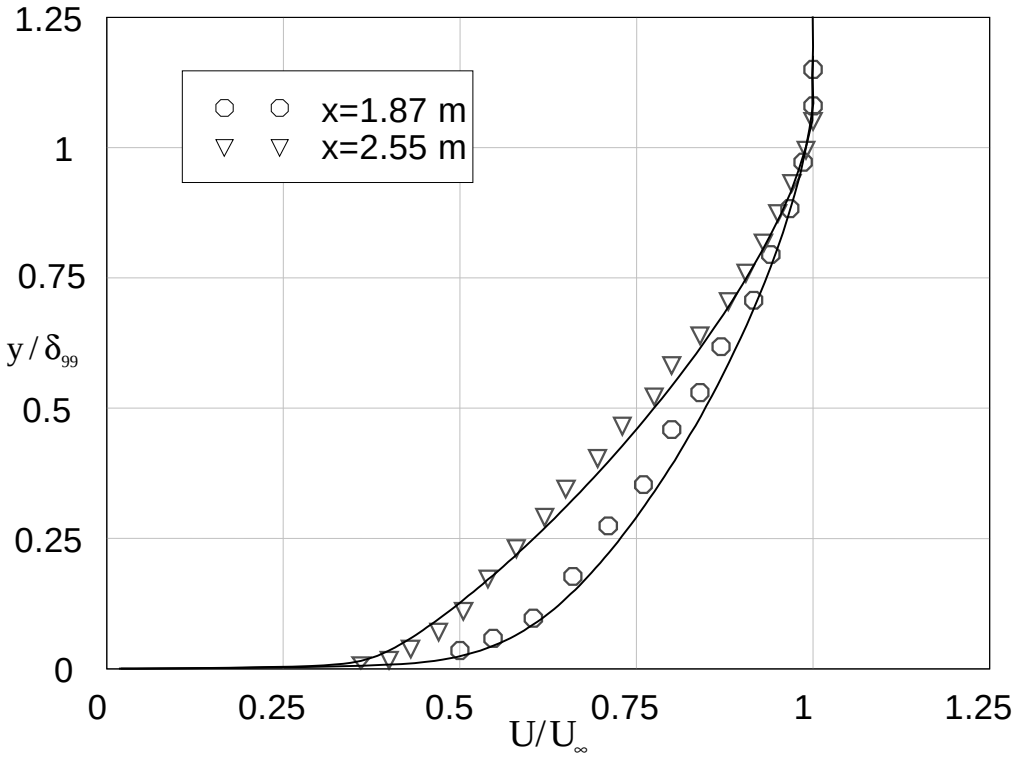

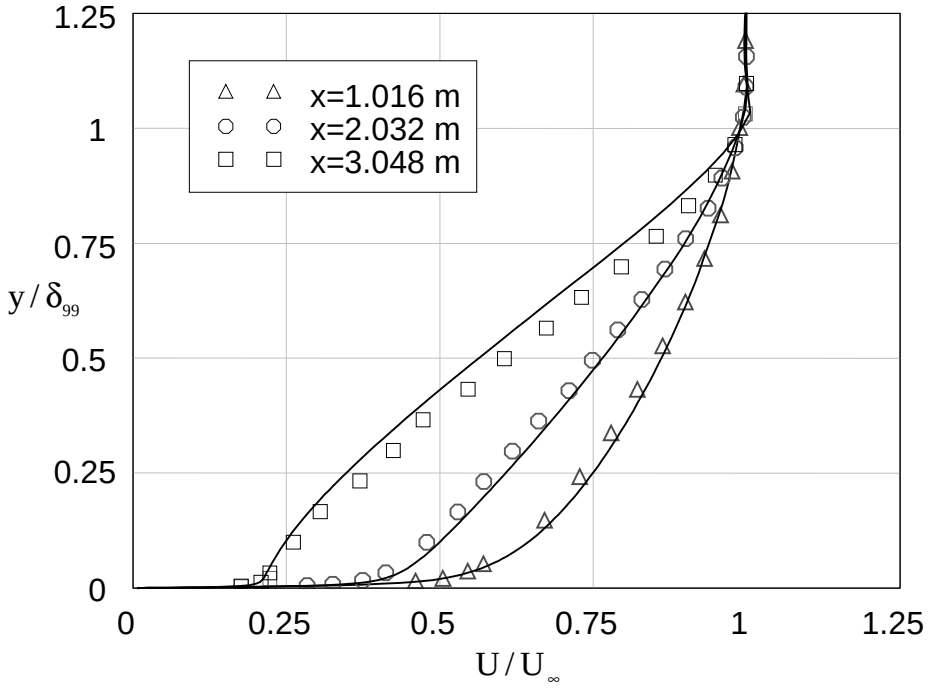

Figure 7: Perot ; Physics of Fluids

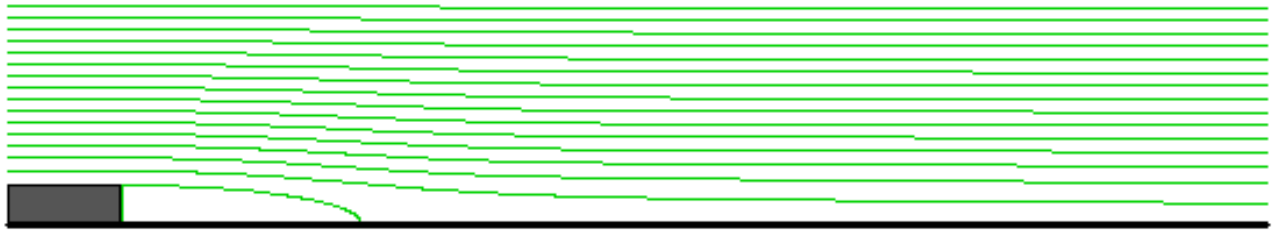

Figure 8: Perot ; Physics of Fluids

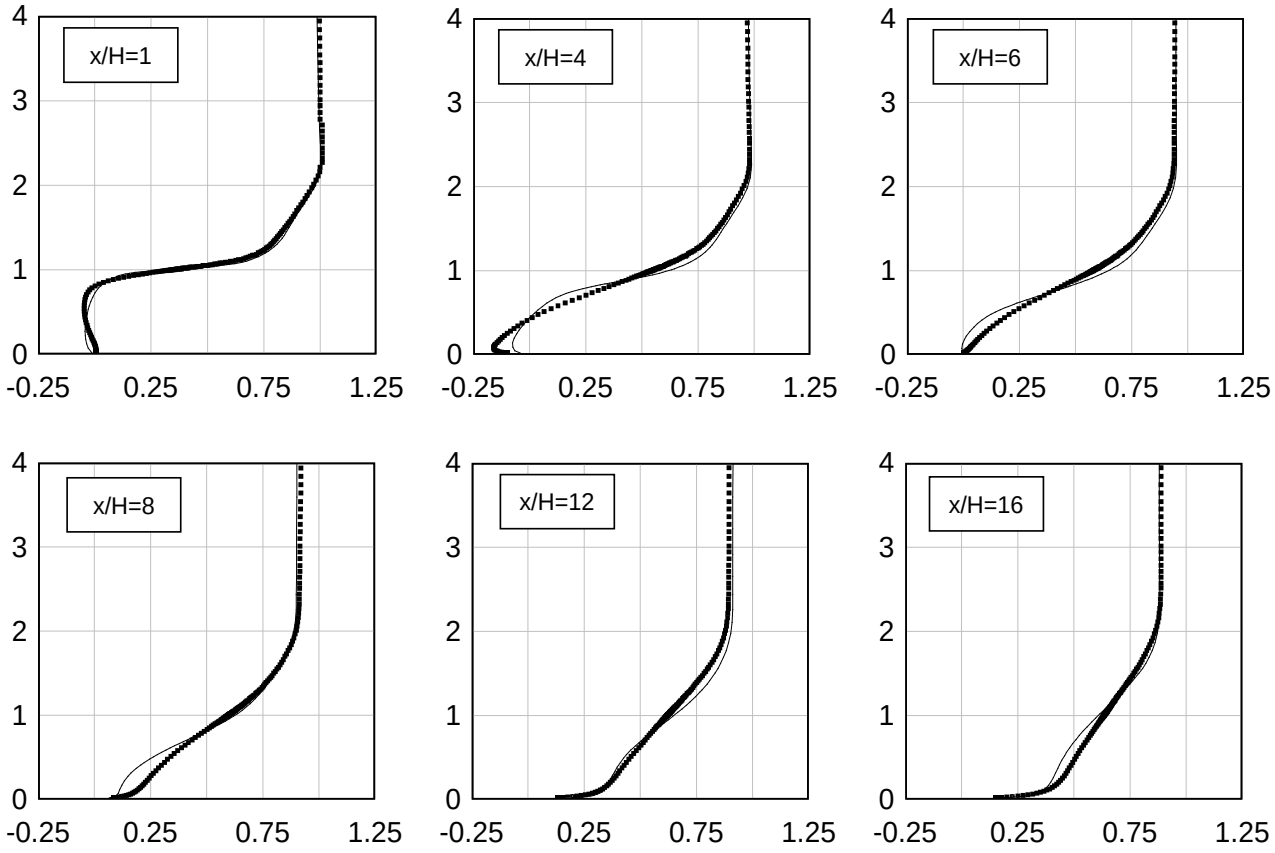

Figure 9: Perot ; Physics of Fluids

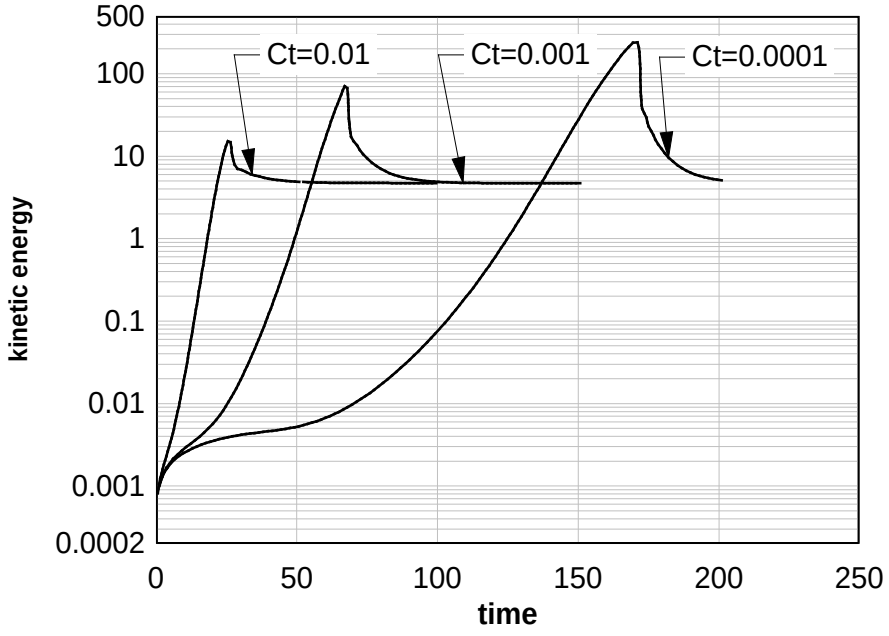

Figure 10 Perot ; Physics of Fluids